

## HOLOGRAPHIC INTERFEROMETRY AS A TOOL FOR VISUALIZATION OF TEMPERATURE FIELDS IN AIR

Petra Dančová<sup>\*,\*\*</sup>, Tomáš Vít<sup>\*,†</sup>, Vít Lédl<sup>†,‡</sup>,  
Zdeněk Trávníček<sup>\*</sup>, Roman Doleček<sup>†,‡</sup>

*Measurement of temperature field in moving fluids is connected with many difficulties. Usage of point temperature measurement methods, such as Constant Current Anemometry (CCA), is limited to frequencies up to 3kHz. This frequency should be the limiting factor for using the CCA in fluid when fast change of temperature occurs. This shortcoming of CCA measurements should be overcome by using of optical methods such as Digital Holographic Interferometry (DHI). It is necessary to employ a special holographic setup with double sensitivity instead of the commonly used Mach-Zehnder type of holographic interferometer in order to obtain the parameters sufficient for the studied cases. This setup is not light efficient like the Mach-Zehnder type but has double sensitivity. The article also shows the method of synchronization and the method for phase averaging of the acquired data. The presented DHI is based on a modified Twyman-Green setup.*

Keywords: Digital Holographic Interferometry (DHI), temperature fields, Mach-Zehnder holographic interferometer, Twyman-Green interferometer

### 1. Introduction

For temperature field measurement, especially in fast moving fluids with high temperature and velocity gradients like pulsatile jets, it is necessary to use a contactless, non-invasive and precise experimental method. Digital holographic interferometry (DHI) follows the above-mentioned criteria. Its whole-field, non-invasive, and differential technique is used for a wide range of applications in industry and research.

In DHI at least two holograms  $h_1$ ,  $h_2$  of wavefronts (one in an initial state and the second one after the change of a temperature field) have to be recorded by a digital sensor. Digital holograms are interference patterns formed by a reference wave and the wave which propagates through the area of interest (measured temperature field). Let's assume that the temperature field is located at a distance  $d$  far from CCD. The numerical reconstruction of the field is calculated by multiplication of digital holograms  $h_i$  with the complex amplitude of the reference wave  $r^*$ . Optical fields in the image plane  $U_i$  are calculated by the Sommerfeld formula which describes the diffraction of a light wave at the hologram in distance  $d$  far

\* Ing. P. Dančová, Ph.D., Ing. Z. Trávníček, CSc., Institute of Thermomechanics AS CR, v.v.i., Doležalkova 5, 188 00 Praha 8

\*\* Ing. P. Dančová, Ph.D., doc. Ing. T. Vít, Ph.D., Technical University of Liberec, Faculty of Mechanical Engineering, Department of Power Engineering Equipment, Studentská 2, 461 17 Liberec 1

† doc. Ing. T. Vít, Ph.D., Ing. V. Lédl, Ph.D., Ing. R. Doleček, TOPTEC, Institute of Plasma Physics AS CR, v.v.i., Sobotekská 1660, 511 01 Turnov

‡ Ing. V. Lédl, Ph.D., Ing. R. Doleček, Technical University of Liberec, Faculty of Mechatronics, Informatics and Interdisciplinary Studies, Studentská 2, 461 17 Liberec 1

from the hologram. The Sommerfeld integral can be solved by Fresnel approximation which in discrete finite form can be written as [3]:

$$U_i(n \Delta x, m \Delta y) = \frac{e^{-j \frac{2\pi}{\lambda} d}}{\lambda d} \sum_{k=1}^N \sum_{l=1}^M h(k \Delta \xi, l \Delta \eta) r^*(k \Delta \xi, l \Delta \eta) e^{\frac{j\pi}{\lambda d} [(k \Delta \xi)^2 + (l \Delta \eta)^2]} e^{-j 2\pi (\frac{k n}{N} + \frac{l m}{M})} \quad (1)$$

where  $j = \sqrt{-1}$  and  $\lambda$  is the wavelength of the used light,  $n = 1, \dots, N$  and  $m = 1, \dots, M$ . The stored hologram consists of  $N \times M$  discrete values. Physical pixels size of used CCD is  $\Delta \xi \times \Delta \eta$ . The equation (1) can be solved effectively by the FFT-algorithm. Intensity  $I$  and phase  $\varphi$  distributions are determined by:

$$I_i(n, m) = |U_i(n, m)|^2, \quad \varphi_i(n, m) = \arctan \left( \frac{\text{Im}(U_i(n, m))}{\text{Re}(U_i(n, m))} \right). \quad (2)$$

If those two digital holograms are individually reconstructed (1) and their phase distributions are calculated (2), then the interference phase can be determined in a pointwise manner by a modulo  $2\pi$  subtraction [1].

Relation between the interference phase and a refractive index change is given by the integral:

$$\Delta \varphi(x, z) = \frac{2\pi}{\lambda} \int_{L_1}^{L_2} \Delta n(x, z, y) dy \quad (3)$$

where  $\Delta n(x, z, y) = n(x, z, y) - n_0$ ,  $n_0$  is refractive index of surrounding air and  $L_2 - L_1$  is length of the beam path in the measured environment. Combining the Gladstone-Dale relation, which relates the index of refraction to the density of a gas, with the ideal gas equation one could get the dependence of the refractive index on the temperature [1, 2]. The key quantity is the density  $\rho$  of the gas:

$$n - 1 = K \rho \quad (4)$$

where  $K$  is the Gladston-Dale constant and  $\rho$  is the density, which are the properties of the gas and  $n$  is refractive index. Principle and main steps of measurement are visible at Fig. 1.

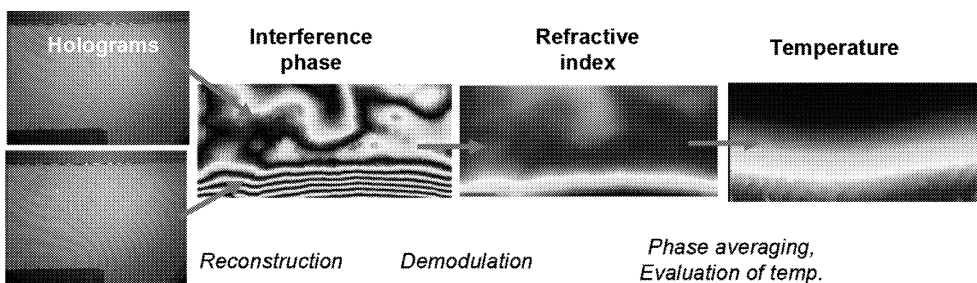


Fig.1: Steps for measurement of the temperature field by digital holographic interferometry

DHI is used for measurement of temperature field of air generated by pulsatile jets in presented study. For measurement of properties of a pulsatile jet, DHI is very suitable, as it can show entire 2D or 3D temperature distribution. For measurement of transparent objects ‘phase objects’, a Mach-Zehnder holographic interferometer setup is usually used. Unfortunately, the phase change is quite small in this type of measurement, thus the sensitivity of the usual interferometer is not sufficient. Previous experiments [1, 2] showed the usefulness of an interferometric setup based on a Twyman-Green interferometer. In this setup the light travels through the phase object twice, which brings the double sensitivity of the setup. However, the setup is more complicated to adjust and is not so light-efficient. Setup for DHI used for our experiments is shown at Fig. 2 and the arrangement of the experiment at Fig. 3.

A 150-mW laser beam (Nd<sup>3+</sup>:YAG) is divided by a polarizing beam splitter BS1 equipped with  $\lambda/2$  plates. After division, both beams are filtered by spatial filters SF and then collimated by collimating objectives CO. Apertures placed in front of the collimating objective ensure a final beam diameter of 50 mm. After collimation, beam ‘2’ enters beam splitter BS2. One part of the beam is reflected by the beam splitter while the second part

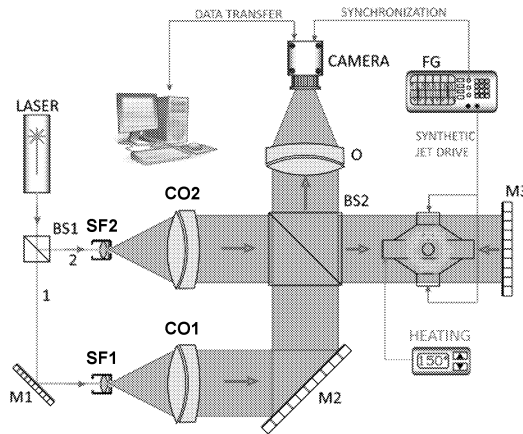


Fig.2: Setup for digital holographic interferometry with double sensitivity (BS – beam splitter, M – mirror, SF – spatial filter, CO – collimating objective, O – focusing objective, FG – function generator)

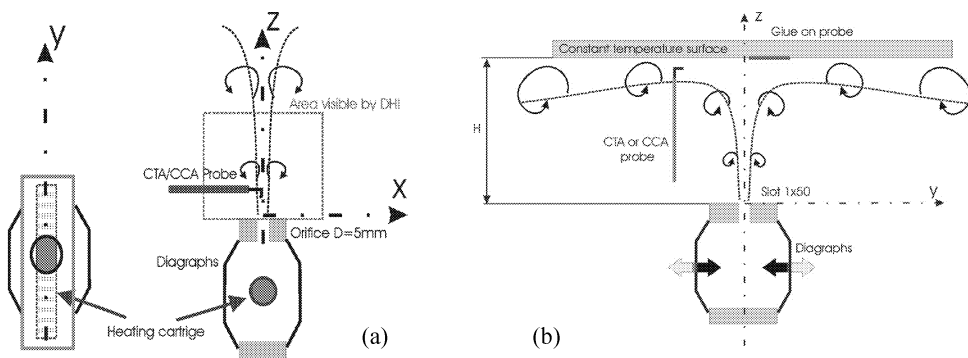


Fig.3: (a) An experimental device, system of coordinates and main dimensions for hot-wire anemometry and holographic interferometry, (b) a schematic view of the pulsed impinging jet setup

travels through the measured object and perpendicularly impinges on mirror M3, where it is reflected and goes through the measured object once more. This is the reason why the interferometer has double sensitivity. Then once again in beam splitter BS2 part of the light is reflected towards the CCD camera and the second part continues in the direction of collimating objective CO2. Beam tagged by '1' (the reference one) after collimation is reflected by mirror M2 towards the CCD camera and goes through beam splitter BS2; both beams impinge the CCD sensor from slightly different directions. The camera and the pulsatile jet are synchronized. However, the setup is more complicated to adjust and is not so light efficient; energy is lost mainly in the beam splitter BS2 (Fig. 2). There are many conditions that must be satisfied or else the functioning of the proposed setup is not feasible. Another problem is the frequency of the phenomenon. In our case of the frequency of the pulsatile jet was 15 Hz. We used AVT Stingray a 5 Mpix camera for hologram recording. We cropped the holograms to  $2048 \times 2048$  pixels. 5 Mpix cameras are still quite slow. The maximum frame rate of AVT Stingray camera in this resolution is approximately 6 FPS. To have a good temporal resolution we would need at least 300 FPS for the 15 Hz frequency (20 samples per period). In the periodic behavior of the pulsatile jet operation we could presume the phenomenon as a quite coherent (every puff is similar). Because of this presumption we could synchronize the camera capture with the certain chosen time within a period (we could make the capture in certain phase of phenomenon). The frame rate of the camera is much slower than the frequency of the phenomenon. Thus it was necessary to ensure that the camera waits till the buffer is empty before another capture is taken, in different phase of the phenomenon. Some periods are usually skipped. This approach has many benefits the most obvious one is that few frames with the same phase could be captured and later averaged. The basic principle of the synchronization method is shown at Fig. 4.

The work uses the term *2D temperature field* representing the projection of the 3D temperature field mean values in the direction of observation.

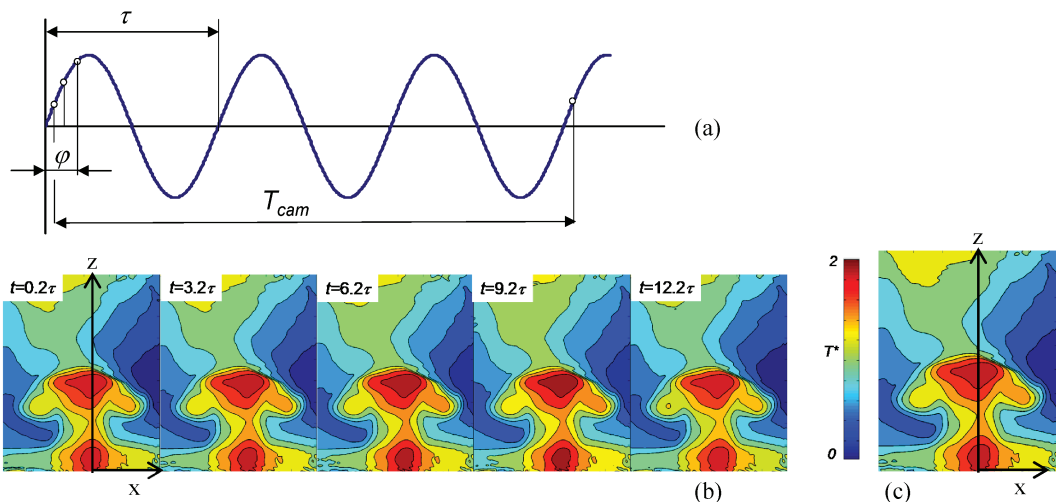


Fig.4: (a) Principle of the synchronization method;  $\varphi$  denotes measured phase,  $T_{CAM}$  denotes the period given by frame rate of the camera, sinusoidal curve denotes the periodic evolution of the measured phenomenon, (b) 2D temperature fields captured on the same phase but at different periods of the phenomenon, (c) phase averaged temperature field

## 2. Experimental setup

The principle of pulsatile jets (PJ) is well described in previous work of authors (see [4, 5]). The main parameters of used PJ are: the mean time orifice velocity  $U_0 = (1/\tau) \int_0^{\tau_E} u_0(t) dt$ , where  $\tau$  is the time period, i.e.  $\tau = 1/f$  and  $f$  is the frequency,  $\tau_E$  is extrusion time ( $\tau_E = T/2$  for the sinusoidal waveform or  $\tau_E \neq T/2$  for the non-sinusoidal waveform),  $u_0(t)$  means the periodical axial orifice velocity and non-dimensional temperature  $T^*$  is defined as:  $T^* = (T - T_a)/(T_0 - T_a)$ , where  $T$  is a temperature of the fluid,  $T_a$  is a temperature of surrounding and  $T_0$  is an average temperature at the nozzle.

Fig. 5 shows time development of the velocity (right side, measured by constant temperature anemometry – CTA) and temperature (left side, measured with constant current anemometry – CCA) fields in plane  $y = 0$ . Figure shows development of the single puff at frequency of oscillations  $f = 15$  Hz. The development of velocity and temperature fields as well as motion of coherent structures is evident.

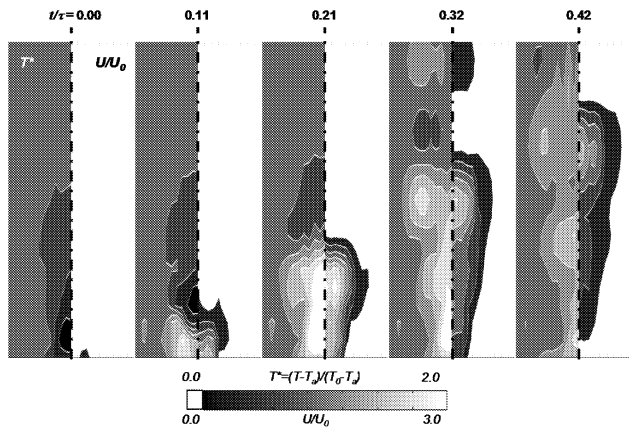


Fig.5: Velocity (right side) and temperature (left side) fields at plane  $y = 0$  at different phase during the cycle  $t/\tau$  measured by CTA/CCA; the velocity field on  $+x$ ,  $+z$  quadrant was measured due to the symmetry of the setup

### 2.1. Pulsatile Jet

Pulsatile Jet actuator consists of a sealed cavity, which is equipped with an emitting orifice (diameter  $D = 5$  mm) and a pair of electrodynamically actuating diaphragms running in opposite directions (diameter  $D_D$  was equal to 53 mm); originating from two ARN-100-10/4 loudspeakers of diameter 94 mm, with nominal electrical resistance  $4 \Omega$ . The orifice is oriented vertically upwards. Experimental setup of PJ is shown on Fig. 3(a). The working fluid is air. The OMEGALUX CIR-10301/240 V Cartridge Heater was equipped with K-type thermocouple and placed into the holder tube inside the actuator cavity. It is possible to control the temperature  $T_c$  of the heating cartage surface up to  $200^\circ \text{C}$  by a connected PID regulator during experiments. The uncertainty of the temperature of the wall was less than  $0.2$  K during single experiment.

### 2.2. Impinging pulsatile jet

Figure 3(b) shows a schematic view of the actuator cavity and the configuration tested in this study. The actuator consists of a cavity which is equipped with an emitting slot

(length  $L$  was equal to 50 mm; width  $s$  was equal to 1.0 mm; corresponding characteristic diameter  $D$  was equal to 2 mm) and a pair of electrodynamically actuating diaphragms running in opposite directions (diameter  $D_D$  was equal to 53 mm; originating from two ARN-100-10/4 loudspeakers of diameter 94 mm, with nominal electrical resistance  $4\ \Omega$ ). The orifice is oriented vertically upwards to the exposed surface of area  $0.13 \times 0.13$  m. The working fluid is air.

The exposed surface was an aluminum plate heated by an Omega KH-505/5-P kapton insulated flexible heater. The temperature of the surface was measured by a K-type thermocouple which was placed on the exposed side of the wall and controlled by a connected PID regulator. The uncertainty of the set temperature of the wall was less than 0.2 K. To enable measurements in different positions the actuator was traversed in the  $y$ -direction under the wall.

Based on an analysis of the velocity field above the actuator [1] the distance between the surface and the slot  $H$  was set to 25 mm in all of the experiments (which corresponds to  $H/D$  equal to 12.5). The input power of the loudspeakers was set to 10 W, the temperature of the surface was  $70\ ^\circ\text{C}$  and held constant during all experiments. The frequency of the oscillations was set to  $f = 1/\tau = 30$  Hz.

The velocity and temperature fields in the vicinity of the surface were measured by a DANTEC Stream Line system with two CTA modules and one CCA module. The temperature field was simultaneously measured with DHI.

A DANTEC 55P14  $90^\circ$ -wire probe operating in constant temperature mode was used to measure velocity magnitude; a DANTEC 55P31 resistance thermometer operating in constant current mode was used to measure temperature. The sampling frequency and number of samples were 6 kHz and 8192, respectively.

### 3. Results

#### 3.1. Pulsatile jet

Figure 6 shows a comparison of 2D temperature fields acquired by DHI (left side of each picture) and CCA (right side of each picture). The pictures correspond to different phase during the cycle  $t/\tau$ . The development of the 2D structure is clearly visible. Fig. 6 illustrates the ability of DHI to visualize 2D temperature field. The position and development of large coherent structures, which puff from the orifice, is evident. It must be noted that in 2D cases, DHI integrates the phase change along the entire path of the rays going through the measured area (through the  $y$  axes), and the results must be presented as the average temperature in the  $y$  direction. The Abel transformation could be used to partially solve this problem. More sufficient is the application of a tomographic approach.

#### 3.2. Impinging pulsatile jet

Figure 7 shows a comparison of the temperature distribution from the DHI and hot wire anemometry (HWA) experiments. It must be mentioned that the data from DHI were acquired at frequency 600 Hz (i.e. 20 pictures/cycle) and are not phase averaged. The results from HWA were acquired at frequency 6000 Hz (i.e. 200 samples/cycle) and are phase averaged as described above. The different phase averaging and uncertainty in phase (temperature) reconstruction of DHI should explain the differences in the presented temperature

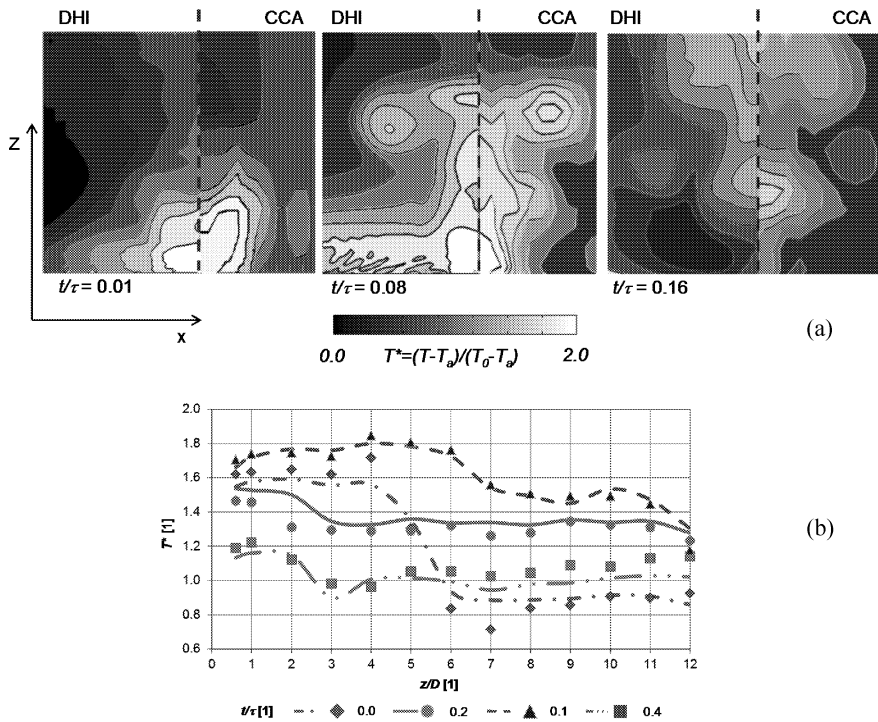


Fig.6: (a) Temperature field above the jet. Images at different  $t/\tau$  achieved by digital holographic interferometry and CCA. The development of the jet is clearly visible from figures. Results from DHI represents average temperature field in  $y$  direction. Results from CCA are achieved at  $y = 0$ . (b) Comparison of temperatures achieved by digital holography interferometry (solid lines) and hot wire anemometry in CCA mode (points) in a stream-wise direction. The results from DHI show the average temperature in the  $y$  direction. The HWA results were achieved at  $y = 0$ .

field. However, the character of the temperature field and its time development are comparable. Figure 7 also illustrates the development of the velocity field measured in constant temperature anemometry (CTA) mode. The position and development of large coherent structures, which puff away the hot air from the surface, is evident.

#### 4. Conclusion

Digital holographic interferometry is very sensitive to noise and needs a sophisticated procedure and software to evaluate the results. Also the usually not high enough frame rate of the cameras could be limiting in many applications. Both of the problems are addressed by the presented method. Well synchronized camera capture time with the phase of observed phenomenon is the key in coherent phenomenon measurement. Such wisely done synchronization brings the benefit of fast developing phenomenon measurement (some frames might be skipped between the exposures of the camera). The series of the images having the same phase (meant in time of the phenomenon development) could be captured and later averaged. The presented results show strength of the implementation of phase averaging to DHI. The third great benefit of the method not researched in this paper is the possibility of obtaining the data suitable for topographic reconstruction.

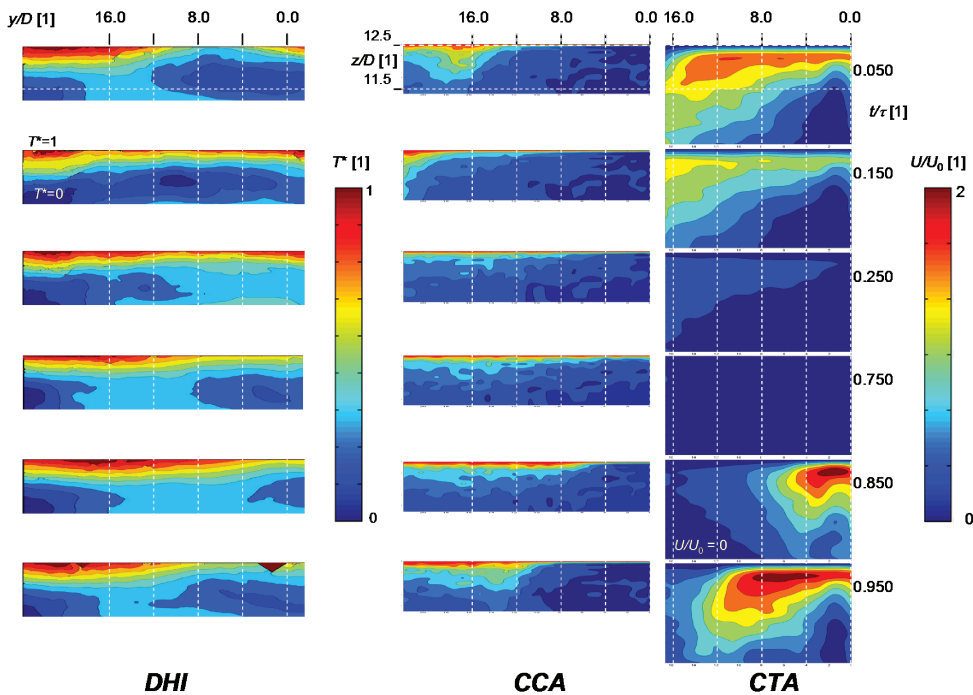


Fig.7: Comparison of velocity and temperature field achieved by holographic interferometry (DHI) and hot-wire anemometry (temperature in CCA mode and velocity in CTA mode); the time scale in presented picture is not uniform

## Acknowledgement

We gratefully acknowledge the support of the GAAS CR (No. IAA200760801), GACR (No. P101-11/J019), the European Regional Development Fund and the Ministry of Education, Youth and Sports of the Czech Republic in the Project No. CZ.1.05/2.1.00/03.0079: Research Center for Special Optics and Optoelectronic Systems (TOPTEC) and SGS 2823.

## References

- [1] Vít T., Lédl V.: Identification of the temperature field in pulsatile impinging flow, In AIP Conference Proceedings 1281, 2010, pp.135–138
- [2] Doleček R., Lédl V., Kopecký V., Psota P., Václavík J., Vít T.: Prospects of digital holographic interferometry in heat transfer measurement, In Experimental Fluid Mechanics 2009, 2009, pp. 25–33
- [3] Kreis T.: Handbook of Holographic Interferometry: Optical and Digital Methods, Berlin: Wiley, 2004
- [4] Kercher D.S., Lee J.-B., Brand O., Allen M.G., Glezer A.: Microjet cooling devices for thermal management of electronics. In IEEE Transactions on Components and Packaging Technologies 26 (2), 2003, pp. 359–366
- [5] Trávníček Z., Hyhlík T., Maršík F.: Synthetic jet impingement heat/mass transfer, In Journal of Flow Visualization and Image Processing, Vol. 13, 2005

Received in editor's office: August 31, 2012

Approved for publishing: October 1, 2013